nature structural & molecular biology

Supplementary information

https://doi.org/10.1038/s41594-025-01738-8

Cereblon induces G3BP2 neosubstrate degradation using molecular surface mimicry

In the format provided by the authors and unedited

Supplementary Information

$CRL4^{CRBN}$ induces G3BP2 neosubstrate degradation using a molecular surface mimicry mechanism

Stefano Annunziato[1,2], Chao Quan[1,2], Etienne J. Donckele[1,2], Ilaria Lamberto[1], Richard D. Bunker[1], Mary Zlotosch[1], Laura Schwander[1], Anastasia Murthy[1], Lars Wiedmer[1], Camille Staehly[1], Michelle Matysik[1], Samuel Gilberto[1], Despina Kapsitidou[1], Daric Wible[1], Gian Marco De Donatis[1], Peter Trenh[1], Rohitha SriRamaratnam[1], Vaik Strande[1], Raphael Lieberherr[1], David Lyon[1], Danielle Steiner[1], Joao Silva[1], Reinaldo Almeida[1], Elena Dolgikh[1], Bradley DeMarco[1], Jennifer Tsai[1], Amine Sadok[1], Vladislav Zarayskiy[1], Magnus Walter[1], Ralph Tiedt[1], Kevin J. Lumb[1], Debora Bonenfant[1], Bernhard Fasching[1], John C. Castle[1], Sharon A. Townson[1], Pablo Gainza[1,*], Georg Petzold[1,*]

[1] Monte Rosa Therapeutics Inc., 321 Harrison Avenue, Suite 900, Boston, MA 02118, USA.

[2] These authors contributed equally to this work.

[*] Correspondence and requests for materials should be addressed to pgainza@monterosatx.com or gpetzold@monterosatx.com.

Supplementary Methods

Global Proteomics Data Acquisition and Analysis

MS1 scans were acquired at resolution 120,000 with 400-1400 mass over charge (m/z) scan range, Automatic Gain Control (AGC) target 4 x 10^5, maximum injection time 50 ms. Then, MS2 precursors were isolated using the quadrupole (0.7 m/z window) with AGC 1 x 10^4 and maximum injection time 50 ms. Precursors were fragmented by collision-induced dissociation (CID) at a normalized collision energy (NCE) of 35% and analyzed in the ion trap. Following MS2, synchronous precursor selection (SPS) MS3 scans were collected by using high energy collision-induced dissociation (HCD) and fragments were analyzed using the Orbitrap (NCE 55 %, AGC target 1 x 10^5, maximum injection time 120 ms, resolution 60,000). Protein identification and quantification were performed using Proteome Discoverer 2.5.0.400 with the SEQUEST algorithm and UniProt human database (2019, 20602 protein sequences). Mass tolerance was set at 10 ppm for precursors and at 0.6 Da for fragments. A maximum of 2 missed cleavages were allowed. Methionine oxidation was set as dynamic modification, while TMT tags on peptide N termini/lysine residues and cysteine alkylation (+113.084) were set as static modifications. Adjustment of reporter ion intensities for isotopic impurities according to the manufacturer's instructions was performed in Proteome Discoverer. Subsequently, protein identifications are inferred from unique peptides, i.e. peptides matching multiple protein entries are excluded. Protein relative quantification is performed using an in-house developed software in Python and R. This analysis included multiple steps; de-duplication of PSMs to peptide charge modification (PCM) level using the average, the sum and the maximum abundance of TMT channels to sort and pick the best PCM, addition of 1 to abundances of PCMs (for all channels) if any of the abundance values is below 0 (for subsequent log2 transformation). MSstatsTMT[59,60] is used for global normalization of TMT channels (equalize medians), to normalize PCMs (for all channels) and summarize protein abundances using Tukey's Median Polish, missing values are imputed using maxQuantileforCensored=NULL. As an intermediate step, before protein summarization, a custom algorithm is applied to find outliers of imputed values (cases where the model fails), and all PCMs for the given protein are reset to being missing. To assess statistical significance, LIMMA's[61,62] linear modeling and

empirical Bayes moderation were applied using default parameters. P-values were computed with moderated t-statistics, and adjusted for multiple testing using Benjamini-Hochberg False Discovery Rate with the topTable function. An arbitrary L2FC cut-off of -1 and +1 is applied to the dataset corresponding to a minimal -50% depletion (x0.5) or +100% enrichment (x2) respectively. The p-value cut-off for statistical significance is set at the standard 10-2 value.

Computational pipeline

Surface computation and visualization

All the surface methods apply in this paper are minimally modified from those presented before[25], and all the computer code is the same presented therein and publicly available. The MaSIF program[40,49] was used to compute all surfaces used in the paper, including electrostatics. MaSIF uses the PyMesh library[63] to process surface meshes, and Adaptive Poisson-Boltzmann Solver (APBS)[64] to compute electrostatics.

1.Definition of buried surface areas

We used the definition of buried surfaces (i.e. the interface of a PPI) identical to that presented elsewhere[40,49]. Under our definition, surface vertices belonging to that buried surface are those that are part of the molecular surface in the unbound structure but buried in the bound structure. PyMesh was applied to regularize the meshes at 1.0 Å resolution. The buried surface of a subunit in a complex structure was calculated by comparing surface vertices of the subunit's surface mesh and the complex's surface mesh. Vertices in the subunit's mesh were labeled as 'interface' meshes if they were more than 2.0 Å away from any complex surface vertex. Once vertices are labeled, the areas of buried regions in the PPI are computed using the vertex area calculator in the PyMesh[63] library. To compute the areas belonging to CULT, MGD or LON domains (**Extended Data Figure 10** and **Figure 5**), we compute the closest atom to each vertex and assign accordingly to CULT, MGD or LON if the closest atom belongs to one of these. We note that the surface areas computed using our approach are typically lower than solvent accessible surface (SAS) areas reported using other methods, as the SAS is larger than the molecular surface and SAS areas usually count the buried region in both sides of the interface while we count only on one side.

2.Prediction of CRBN PPI propensity

The MaSIF-site program[40] was used to compute a per-vertex propensity of the G3BP2 NTF2L surface (PDB: 5drv) to become buried in a PPI, as visualized in **Figure 1** or the propensity of surface vertices in closed CRBN to become buried in a PPI taken from the PDB entry 5fqd, with all ligands removed (shown in **Extended Data Figure 1**). MaSIF-site uses as input the per-vertex chemical and geometrical features projected on the surface of a protein, and uses them to compute a score for each vertex shown to correspond to its propensity become buried in a protein-protein interaction[40]. MaSIF-site is built on a geometric deep learning architecture trained to predict the buried surface from a training set of thousands of proteins. The training set did not contain any G3BP2 or G3BP1 proteins. For visualization purposes, the propensity of each vertex, computed as a real value between 0 and 1, was display as a regression, from blue to white to red.

3.Surface matching of the USP10 – CRBN similarity

The MaSIF-seed program[40,49] is a surface matching pipeline that uses geometric deep learning to encode surface patches as fingerprints. MaSIF-seed was designed and tested to match surfaces that are complementarity to each other based on their fingerprint, followed by an alignment step. MaSIF-seed was modified to match patches by similarity (or *mimicry*) instead of complementarity.

4.Overall method description of MaSIF-seed

MaSIF-seed[49] method is a geometric deep learning approach designed to identify complementary structural motifs that can mediate protein-protein interactions. It works by analyzing protein molecular surfaces, which are divided into overlapping radial patches, to capture both chemical and geometric features relevant to binding. Every vertex on the surface becomes the center of its own radial patch of radius 12 Å. A neural network is then trained to generate "fingerprints" for these overlapping surface patches that predict their binding propensity. MaSIF-seed uses this fingerprint matching process to find complementary surface motifs from a large database of potential binding partners. The MaSIF-seed method involves an important alignment step after the initial identification of complementary surface motifs. Once the surface patches from the target and potential binding seeds are

matched based on their fingerprints, these patches are aligned geometrically to evaluate how well they fit together. A second neural network, called the interface post alignment (IPA) score network is used to score the aligned surface patches specifically for complementarity.

5.Definition of the USP10 interfaces as a surface patch.

A structure of USP10 bound to G3BP2 NTF2L is not available, but there is one of G3BP1 NTF2L in the presence of USP10 (PDB: 7xhf). Since the USP10 interface is highly conserved in G3BP1 and G3BP2, we built a simple model of G3BP2 NTF2L bound to USP10 by aligning the G3BP2 NTF2L structure (PDB: 5drv) to the G3BP1 NTF2L in its structure with USP10 (PDB: 7xhf) and then removing G3BP1. The molecular surfaces of USP10 from its co-crystal structures with G3BP1 NTF2L was used as input to the algorithm. The buried surface in the G3BP1:USP10 complex was computed as described above. The interface patch was defined as the patch of radius 12 Å that captures the largest area of the USP10:G3BP1 region. The G3BP2 NTF2L in the model was used only for clashing computation purposes.

6.Modification of MaSIF-seed for surface similarity

MaSIF-seed was modified to match and align similar surface patches instead of complementary patches. MaSIF-seed by default inverts the input features and normals of the target patch to align for complementarity, but this is no longer required for similarity matching. To align patches by similarity, these features were no longer inverted. MaSIF-search fingerprints were computed for all the patches decomposed from the molecular surfaces of the CRBN closed conformation (PDB: 5fqd). In the first stage, patches with fingerprints and an Euclidean distance greater than 2.5 units in the embedding space were discarded. Patches that passed this filter were selected for a second stage alignment step. Since every vertex in the surface is the center of a patch, each vertex on the surface has a computed fingerprint. In the second stage alignment step, the RANSAC algorithm is used to perform an alignment between the patches of CRBN and those of USP10. In each iteration of RANSAC three vertices in the matched patch are randomly selected, and the most similar fingerprint in the query patch (USP10) are identified. The three matches are used to perform an alignment and the number of inlier vertices after the alignment is used to initially score the alignment. The alignment with the highest number of inliers

is accepted. Finally, a scoring of similarity is performed using the scored fingerprints. Specifically, after an alignment all vertices of the aligned patch within a 3D distance of 2.0 Å from a vertex in the query patch are selected. The fingerprint distance *d* is computed between the selected vertices and each of the corresponding nearest neighbor's fingerprint in the query patch. The score for the alignment is computed as $\sum_{ij} 1/d_{ij}^2$ such that i is the vertex in the aligned patch and j is the vertex in the query patch and d is the fingerprint Euclidean distance. The interface post-alignment (IPA) scoring neural network [49] was set to a small value (0.50). MaSIF-seed contains a steric, atomic based post-processing filter which is used by default to filter matched results for steric compatibility with the complementary target. Since similarity was performed here, the input was modified so that the steric filter comparison is performed against G3BP2 in the model, removing any solution where no steric clashes involving Cα atoms were allowed, and up to 10 clashes involving other heavy atoms were allowed.

7.Computation of surface similarity

To visually display the surface similarity of CRBN and USP10 for representation in **Fig. 1**, after the surface-based alignment and scoring, a per-surface-vertex surface similarity was computed on the surfaces after alignment by the algorithm. The surface similarity score was computed in the same way that per-vertex shape complementarity has been previously defined [65]. Let A and B be two proteins aligned under our surface alignment algorithm. Let P_A be the molecular surface of protein A, and x_A be a vertex on the surface of A with normal n_A. Let P_B be the molecular surface of protein B, and x'_A be the point on the surface of B closest to x_A with normal n'_A .Then, the surface similarity for vertex x_A is defined as:

$$S^{A\to B}(x_A) = (n_A.n'_A)\exp\left[-w(|x_A - n'_A|)^2\right],$$

where w=0.25.

To provide a visual contrast with other surfaces and help the readers visualize surface similarity, we selected a CRBN F150A mutant as a counter example. Since using the masif-based methods on CRBN F150A did not produce a similar pose to that of wildtype CRBN, we structurally aligned CRBN F150A to the predicted CRBN

pose and computed both its fingerprint similarity score (see preceding section) and its per-point surface similarity.

Calculation of low energy conformations of MRT-5702 Stereoisomers

Ligand conformation generation was carried out with OMEGA[66] version 5.1.0 (10.1021/ci100031x) with Ewindow of 10 kcal/mol and Maxconfs of 800. The four different enantiomers of MRT-5702 were submitted as SMILES strings to OMEGA to avoid carry-over of conformation information before the calculations. MRT-5702 shares the chemical substructure of 1-(imidazo[1,2-a]pyridin-3-yl)dihydropyrimidine-2,4(1H,3H)-dione with that of MRT-3486 in the ternary complex x-ray structure between CRBN-DDB1 and NEK7 (PDB: 9nfq), which binds the tri-Trp pocket of CRBN and served as a template for ligand alignment. To this end, the position of this chemical substructure was extracted from 9nfq after superposition with the CRBN-DDB1 model derived from the cryo-EM map of MRT-5702 (aligned via CRBN residues 380, 386+ and 400). The pose of the extracted chemical substructure was energetically minimized within the CRBN pocket of the Cryo-EM model using Maestro version 14.0 to remove potential model bias from 9NFQ. The generated conformers of MRT-5702 were aligned to the minimized 1-(imidazo[1,2-a]pyridin-3-yl)dihydropyrimidine-2,4(1H,3H)-dione moiety using RDKit version 2024.03.5 (www.rdkit.org). Aligned conformers were assessed by PoseBusters[67] for clashes with the cryo-EM model of CRBN-DDB1 or G3BP2 by calculating volume overlaps between ligands and the protein model. Ligand conformers with volume overlaps greater than 7.5% were discarded[67]. The remaining conformers of all four MRT-5702 stereoisomers were scored according to their ligand volume overlap with the experimental cryo-EM map by calculating the SMOC score (segment-based Manders overlap coeff.)[68]. The SMOC score is calculated as implemented in the python package of TEMPy[69] version 2.0.0 on the full Cryo-EM map and plotted for each stereoisomer using seaborn[70].

Chemical synthesis of MRT-5702

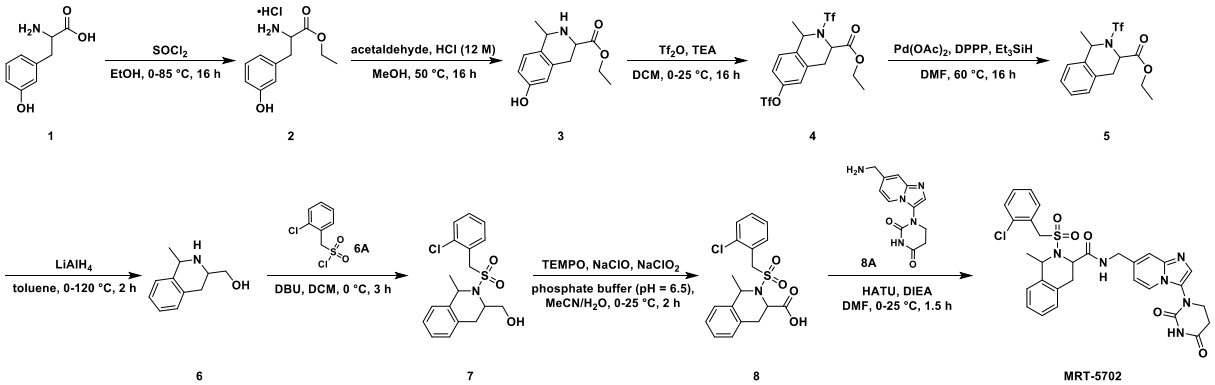

Scheme 1: Synthesis of **MRT-5702**

To a suspension of 2-amino-3-(3-hydroxyphenyl)propanoic acid (**1**) (10.0 g, 55.2 mmol, 1.00 *eq*) in ethanol (100 mL) was added dropwise sulfurous dichloride (15.1 g, 127 mmol, 9.22 mL, 2.3 *eq*) at 0 °C. The mixture was stirred at 85 °C for 16 h. The mixture was concentrated under reduced pressure to give intermediate **2** (15.0 g, crude) as yellow oil. A mixture of crude material **2** in methanol (250 mL) was added acetaldehyde (30.4 g, 276 mmol, 38.7 mL, 40% purity, 5.00 *eq*) and hydrochloric acid (12 M, 13.8 mL, 3.00 *eq*). The mixture was stirred at 50 °C for 16 h. The mixture was concentrated under reduced pressure to give a residue. The residue was triturated with a solution of petroleum ether/ethyl acetate (5/1, 200 mL) at 25 °C for 2 h. The mixture was filtered, and the filter cake was washed with petroleum ether (50 mL). The filter cake was collected and dried under reduced pressure to give compound **3** (9.3 g, 39.7 mmol, 72% yield) as a white solid.

Compound **3**: ^{1}H NMR (400 MHz, DMSO-d_6) δ = 9.90 - 9.46 (m, 2H), 7.15 - 7.03 (m, 1H), 6.75 - 6.68 (m, 1H), 6.65 - 6.60 (m, 1H), 4.61 - 4.43 (m, 2H), 4.33 - 4.19 (m, 2H), 3.28 - 3.16 (m, 2H), 1.65 - 1.53 (m, 3H), 1.38 - 1.14 (m, 3H). MS (ESI) m/z 236.1 $[M+H]^+$

To a solution of **3** (9.3 g, 39.7 mmol, 1.00 *eq*) in dichloromethane (70 mL) were added triethylamine (11.9 g, 118 mmol, 16.4 mL, 3.00 *eq*) and trifluoromethanesulfonic anhydride (33.3 g, 118 mmol, 19.4 mL, 3.00 *eq*) at 0 °C. The mixture was stirred at 25 °C for 16 h. The mixture was concentrated under reduced pressure. The crude product was purified by flash silica gel chromatography (ISCO®; 220 g SepaFlash® Silica Flash Column, Eluent of 0~10% Ethyl acetate/Petroleum ether gradient at 80 mL/min) to give compound **4** (6.14 g, 12.3 mmol, 31% yield) as yellow oil.

Compound **4**: ^{1}H NMR (400 MHz, DMSO-d_6) δ = 7.63 - 7.46 (m, 2H), 7.44 - 7.36 (m, 1H), 5.44 - 5.19 (m, 1H), 5.07 - 4.70 (m, 1H), 4.27 - 3.85 (m, 2H), 3.57 - 3.40 (m, 2H), 1.51 (d, *J* = 6.8 Hz, 3H), 1.27 - 0.85 (m, 3H). MS (ESI) m/z 500.0 $[M+H]^+$

To a solution of **4** (5.50 g, 11.0 mmol, 1.00 *eq*) in *N*,*N*-dimethylformamide (50 mL) were added triethylsilane (3.84 g, 33.0 mmol, 5.28 mL, 3.00 *eq*), palladium(II) acetate (494 mg, 2.20 mmol, 0.200 *eq*) and 1,3-bis(diphenylphosphaneyl)propane (908 mg, 2.20 mmol, 0.200 *eq*). The system was purged with nitrogen for three times. The mixture was stirred at 60 °C for 16 h under nitrogen atmosphere. After being cooled to room temperature, the reaction mixture was diluted with water (100 mL) and extracted with ethyl acetate (3 × 100 mL). The combined organic layers were washed with brine (120 mL), dried over anhydrous sodium sulfate, filtered and concentrated under reduced pressure to give a residue. The crude product was purified by reversed phase column (C18, 330 g, flow: 100 mL/min; gradient: from 65-70% water (0.1% formic acid) in acetonitrile over 60 min. to give intermediate **5** (3.22 g, 9.07 mmol, 82% yield) as a yellow solid.

Compound **5**: ^{1}H NMR (400 MHz, DMSO-d_6) δ = 7.39 - 7.15 (m, 4H), 5.29 - 5.08 (m, 1H), 4.98 - 4.63 (m, 1H), 4.25 - 3.85 (m, 2H), 3.31 - 3.15 (m, 2H), 1.58 - 1.43 (m, 3H), 1.29 - 0.84 (m, 3H). MS (ESI) m/z 352.0 $[M+H]^+$

To a suspension of aluminum (III) lithium hydride (3.40 g, 9.68 mmol, 1.00 *eq*) in toluene (40 mL) was added compound **5** (2.5 M, 19.4 mL, 5.00 *eq*) at 0 °C under nitrogen atmosphere. The mixture was stirred at 120 °C for 2 h under nitrogen atmosphere. The mixture was cooled to 0 °C and was quenched with water (2 mL) followed by 15% sodium hydroxide solution (2 mL) and water (6 mL) at 0 °C. The reaction mixture was diluted with water (80 mL) and extracted with ethyl acetate (3 × 80 mL). The combined organic layers were washed with brine (100 mL), dried over anhydrous sodium sulfate, filtered and concentrated under reduced pressure to give 1.90g of crude **6** as a white solid. 450 mg of crude **6** (2.54 mmol, 1.00 *eq*) and 1.16g of 2,3,4,6,7,8,9,10-octahydropyrimido[1,2-*a*]azepine (7.62 mmol, 1.15 mL, 3.00 *eq*) in dichloromethane (8 mL) were added to a solution of (2-chlorophenyl)methanesulfonyl chloride **6A** (857 mg, 3.81 mmol, 1.50 *eq*) in dichloromethane (2 mL) dropwise at 0 °C. The mixture was stirred at 0 °C for 3 h. The reaction mixture was concentrated under reduced pressure. The residue was purified by *Prep*-HPLC (column: Waters Xbridge Prep OBD C18 150 × 40 mm × 10

μm; mobile phase: [water (ammonium bicarbonate) - acetonitrile]; gradient: 35%-65% B over 20 min) to give compound **7** (130 mg, 355 μmol, 14% yield) as a yellow solid.

Compound **7**: ^{1}H NMR (400 MHz, $CDCl_3$) δ = 7.58 - 7.40 (m, 1H), 7.35 - 7.29 (m, 2H), 7.26 - 7.15 (m, 4H), 7.14 - 7.02 (m, 1H), 5.04 - 4.88 (m, 1H), 4.64 - 4.41 (m, 1H), 4.25 - 4.11 (m, 1H), 4.01 (q, *J* = 6.4 Hz, 1H), 3.77 (dd, *J* = 2.0, 6.0 Hz, 1H), 3.42 - 3.32 (m, 2H), 3.13 - 2.95 (m, 1H), 2.69 (s, 1H), 1.62 - 1.48 (m, 3H). MS (ESI) m/z 364.2 $[M-H]^-$

To a solution of **7** (130 mg, 355 μmol, 1.00 *eq*) in phosphate buffer (3 mL) and acetonitrile (3 mL) was added 2,2,6,6-tetramethylpiperidinooxy (44.7 mg, 284 μmol, 0.800 *eq*) followed by the solution of sodium chlorite (64.3 mg, 711 μmol, 2.00 *eq*) in water (0.75 mL) and sodium hypochlorite (529 mg, 355 μmol, 439 μL, 5% purity, 1.00 *eq*) in portions at 0 °C. The mixture was stirred at 25 °C for 2 h. The reaction mixture was quenched with 1M hydrochloric acid and the mixture was adjusted to pH = 3-4. Then the mixture was diluted with ethyl acetate (20 mL) and water (20 mL). The layers were separated, and the aqueous phase was extracted with ethyl acetate (2 × 20 mL). The combined organic layers were washed with brine (30 mL), dried over sodium sulfate, filtered and concentrated under reduced pressure to give compound **8** (98 mg, 259 μmol, 73% yield) as yellow oil.

Compound **8**: ^{1}H NMR (400 MHz, $CDCl_3$) δ = 7.64 - 7.43 (m, 1H), 7.33 (d, *J* = 7.6 Hz, 2H), 7.25 - 7.10 (m, 4H), 7.07 - 6.90 (m, 1H), 5.05 - 4.86 (m, 1H), 4.75 - 4.61 (m, 1H), 4.56 - 4.22 (m, 2H), 3.31 - 3.21 (m, 1H), 3.18 - 3.09 (m, 1H), 1.62 - 1.42 (m, 3H). MS (ESI) m/z 378.0 $[M-H]^-$

To a solution of compound **8** (98 mg, 259 μmol, 1.00 *eq*) in *N*,*N*-dimethylformamide (3 mL) was added *N*,*N*-diisopropylethylamine (102 mg, 790 μmol, 138 μL, 3.3 *eq*) followed by *O*-(7-azabenzotriazol-1-yl)-*N*,*N*,*N*′,*N*′-tetramethyluronium hexafluorophosphate (147 mg, 395 μmol, 1.50 *eq*) at 0 °C. After stirring at 0 °C for 30 min, 1-(7-(aminomethyl)imidazo[1,2-*a*]pyridin-3-yl)dihydropyrimidine-2,4(1*H*,3*H*)-dione (27.75 mg, 342.23 μmol, 1.30 *eq*) was added to the mixture. The resulting mixture was stirred at 25 °C for 1 h. The reaction mixture was quenched with water (20 mL) and diluted with ethyl acetate (20 mL). The layers were separated, and the aqueous phase was extracted with ethyl acetate (2 × 20 mL). The combined organic

layers were washed with saturated sodium bicarbonate solution (2 × 30 mL) followed by brine (30 mL), dried over sodium sulfate, filtered and concentrated under reduced pressure. The residue was purified by *Prep*-HPLC (column: Welch Xtimate C18 150 × 25 mm × 5 μm; mobile phase: [water (formic acid) - acetonitrile]; gradient: 10%-40% B over 15 min) and lyophilized to **MRT-5702** (117 mg, 188 μmol, 72.6% yield) as a white solid.

Compound **MRT-5702**: ^{1}H NMR (400 MHz, DMSO-d_6) δ = 10.90 - 10.76 (m, 1H), 8.82 - 8.47 (m, 2H), 8.17 - 7.99 (m, 1H), 7.74 - 7.44 (m, 2H), 7.43 - 7.24 (m, 6H), 7.20 - 6.92 (m, 2H), 5.11 - 4.96 (m, 1H), 4.88 - 4.63 (m, 1H), 4.61 - 4.41 (m, 2H), 4.38 - 4.14 (m, 2H), 3.84 (t, *J* = 6.4 Hz, 2H), 3.20 - 3.06 (m, 2H), 2.85 (d, *J* = 2.0 Hz, 2H), 1.59 - 1.42 (m, 3H). MS (ESI) m/z 621.3 $[M+H]^+$

SFC Separation of MRT-5702

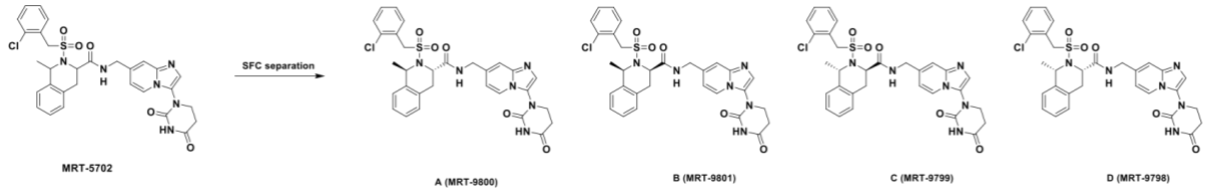

Scheme 2: SFC Separation of MRT-5702. Configuration of MRT-9800 (MRT-5702A) and MRT-9799 (MRT-5702C) determined by X-ray crystallography. The configuration of MRT-9798 (MRT-5702C) was access by modeling and MRT-9801 (MRT-5702B) is the remaining configuration.

MRT-5702 (117 mg, 188 μmol, 1.00 *eq*) was separated by Chiral SFC (column: (s,s) WHELK-O1 (250 mm × 30 mm,10 μm); mobile phase: [carbon dioxide- propan-2-ol / acetonitrile]; B%: 62%, isocratic elution mode) to give Peak 1 and **B**. **B** was purified by *Prep*-HPLC (column: Phenomenex luna C18 150 × 25 mm × 10 μm; mobile phase: [water (formic acid) - acetonitrile]; gradient: 15%-45% B over 1 min). Compound **B** (17 mg, 27 μmol, 14% yield) was obtained as a white solid. Peak1 was separated by Chiral SFC (column: DAICEL CHIRALPAK AS (250 mm × 30 mm, 10 μm); mobile phase: [carbon dioxide - ethanol (0.1% ammonia hydrate)]; B%:40%, isocratic elution mode) to give Peak 2 and **A**. **A** was purified by *Prep*-HPLC (column:

Welch Xtimate C18 150 × 25 mm × 5 μm; mobile phase: [water (formic acid) - acetonitrile]; gradient: 10%-40% B over 15 min). Compound **A** (12 mg, 19 μmol, 10% yield) was obtained as a white solid. Peak 2 was separated by Chiral SFC (column: DAICEL CHIRALCEL OJ (250 mm × 30 mm, 10 μm); mobile phase: [carbon dioxide - ethanol / acetonitrile]; B%: 50%, isocratic elution mode) to give **compounds C** and **D**. **C** was purified by *Prep*-HPLC (column: Welch Xtimate C18 150 × 25 mm × 5 μm; mobile phase: [water (formic acid) - acetonitrile]; gradient: 13%-43% B over 10 min). Compound **C** (10 mg, 16.1 μmol, 8.6% yield) was obtained as a white solid. **D** was purified by *Prep*-HPLC (column: Welch Xtimate C18 150 × 25 mm × 5 μm; mobile phase: [water (formic acid) - acetonitrile]; gradient: 10%-40% B over 10 min). Compound **D** (16 mg, 26.3 μmol, 14% yield) was obtained as a white solid.

Compound **A**: ^{1}H NMR (400 MHz, DMSO-d_6) δ = 10.66 (s, 1H), 8.51 (t, *J* = 6.0 Hz, 1H), 8.13 (d, *J* = 7.2 Hz, 1H), 7.59 (dd, *J* = 2.0, 7.2 Hz, 1H), 7.55 - 7.46 (m, 2H), 7.43 - 7.32 (m, 2H), 7.24 - 7.08 (m, 5H), 6.56 (d, *J* = 7.2 Hz, 1H), 5.04 (q, *J* = 6.8 Hz, 1H), 4.82 (d, *J* = 13.6 Hz, 1H), 4.74 (d, *J* = 3.2 Hz, 1H), 4.61 (d, *J* = 13.6 Hz, 1H), 4.18 (d, *J* = 6.0 Hz, 2H), 3.77 (t, *J* = 6.8 Hz, 2H), 3.45 (dd, *J* = 5.6, 15.6 Hz, 1H), 3.18 - 3.06 (m, 1H), 2.82 (t, *J* = 6.4 Hz, 2H), 1.46 (d, *J* = 6.4 Hz, 3H). MS (ESI) m/z 621.3 $[M+H]^+$

Compound **B**: ^{1}H NMR (400 MHz, DMSO-d_6) δ = 10.65 (s, 1H), 8.59 (t, *J* = 5.6 Hz, 1H), 8.25 (d, *J* = 6.8 Hz, 1H), 7.50 (s, 1H), 7.46 - 7.39 (m, 2H), 7.37 - 7.21 (m, 7H), 6.91 (dd, *J* = 1.2, 7.2 Hz, 1H), 5.01 (d, *J* = 7.2 Hz, 1H), 4.50 - 4.38 (m, 3H), 4.35 (d, *J* = 13.6 Hz, 1H), 4.20 (d, *J* = 13.6 Hz, 1H), 3.78 (t, *J* = 6.4 Hz, 2H), 3.23 - 3.06 (m, 2H), 2.82 (t, *J* = 5.6 Hz, 2H), 1.54 (d, *J* = 7.2 Hz, 3H). MS (ESI) m/z 621.3 $[M+H]^+$

Compound **C**: ^{1}H NMR (400 MHz, DMSO-d_6) δ = 10.66 (s, 1H), 8.51 (t, *J* = 5.6 Hz, 1H), 8.14 (d, *J* = 7.2 Hz, 1H), 7.59 (dd, *J* = 1.6, 7.2 Hz, 1H), 7.54 - 7.47 (m, 2H), 7.43 - 7.33 (m, 2H), 7.25 - 7.09 (m, 5H), 6.58 (d, *J* = 7.2 Hz, 1H), 5.04 (q, *J* = 6.4 Hz, 1H), 4.82 (d, *J* = 13.6 Hz, 1H), 4.74 (d, *J* = 3.2 Hz, 1H), 4.61 (d, *J* = 13.6 Hz, 1H), 4.19 (d, *J* = 6.0 Hz, 2H), 3.77 (t, *J* = 6.4 Hz, 2H), 3.48 - 3.42 (m, 1H), 3.12 (dd, *J* = 2.0, 15.6 Hz, 1H), 2.83 (t, *J* = 6.4 Hz, 2H), 1.46 (d, *J* = 6.4 Hz, 3H).

Compound **D**: ^{1}H NMR (400 MHz, DMSO-d_6) δ = 10.65 (s, 1H), 8.58 (t, *J* = 6.0 Hz, 1H), 8.26 (d, *J* = 6.8 Hz, 1H), 7.51 (s, 1H), 7.47 - 7.38 (m, 2H), 7.37 - 7.21 (m, 7H), 6.92 (dd, *J* = 1.2, 7.2 Hz, 1H), 5.02 (q, *J* = 7.2 Hz, 1H), 4.52 - 4.38 (m, 3H), 4.35 (d, *J* = 13.6 Hz, 1H), 4.20 (d, *J* = 13.6 Hz, 1H), 3.78 (t, *J* = 6.4 Hz, 2H), 3.28 - 3.22 (m,

1H), 3.16 - 3.07 (m, 1H), 2.82 (t, *J* = 5.6 Hz, 2H), 1.54 (d, *J* = 7.2 Hz, 3H). MS (ESI) m/z 621.1 $[M+H]^+$

X-ray

Equipment used for X-ray:

Rigaku Oxford Diffraction XtaLAB Synergy-S equipped with a HyPix-6000HE area detector Cryogenic system: Oxford Cryostream 800

Cu: λ=1.54184 Å, 50W

Distance from the crystal to the CCD detector: d = 35 mm

Tube Voltage: 50 kV; Tube Current: 1 mA

MRT-5702A

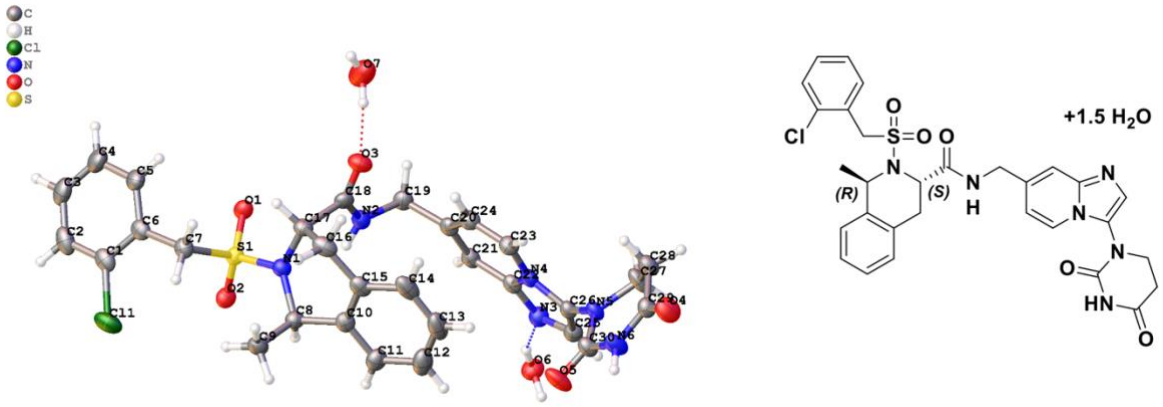

Scheme 3: X-Ray Structure of MRT-5702A (MRT-9800) in (*R,S*) configuration.

The symmetry of the crystal structure was assigned the monoclinic space group C2 with the following parameters: a = 21.3601(3) Å, b = 11.2017(2) Å, c = 12.5762(2) Å, α = 90°, β = 97.521(2)°, γ = 90°, V = 2983.21(8) Å3, Z = 4, Dc = 1.443 g/cm^3, μ(CuKα) = 2.272 mm^{-1}, and F(000) = 1356.0.

Colorless block-shaped single crystals of MRT-5702A were obtained from methanol - water (4:1). A suitable crystal 0.30 × 0.10 × 0.10 mm3 was selected for testing. Data collection temperature: T = 149.99(10) K. Total of 18187 reflections were collected in the 2θ range from 7.09 to 133.17. The limiting indices were: -24 ≤ h ≤ 25, -13 ≤ k ≤ 13, -14 ≤ l ≤ 14; which yielded 5130 unique reflections (Rint = 0.0690). The structure was solved using SHELXT (Sheldrick, G. M. 2015. Acta Cryst. A71, 3-8) and refined using SHELXL (against F²) (Sheldrick, G. M. 2015. Acta Cryst. C71, 3-8). The total number of refined parameters was 408, compared with 5130 data. All reflections were included in the refinement. The goodness of fit on F² was 1.058 with a final R value for [I >= 2σ (I)] R_1 = 0.0368 and wR_2 = 0.0966. The largest differential peak and hole were 0.40 and -0.34 eÅ^{-3}.

Crystal data and structure refinement for EW40755-419-P1B_auto.

Identification code	EW40755-419-P1B_auto
Empirical formula	$C_{30}H_{32}ClN_6O_{6.5}S$
Formula weight	648.12
Temperature/K	149.99(10)
Crystal system	monoclinic
Space group	C2
a/Å	21.3601(3)
b/Å	11.2017(2)
c/Å	12.5762(2)
α/°	90
β/°	97.521(2)
γ/°	90
Volume/Å^3	2983.21(8)
Z	4
ρ_{calc}g/cm^3	1.443
μ/mm^{-1}	2.272

F(000)	1356.0
Crystal size/mm^3	0.3 × 0.1 × 0.1
Radiation	Cu Kα (λ = 1.54184)
2Θ range for data collection/°	7.09 to 133.17
Index ranges	-24 ≤ h ≤ 25, -13 ≤ k ≤ 13, -14 ≤ l ≤ 14
Reflections collected	18187
Independent reflections	5130 [R_{int} = 0.0690, R_{sigma} = 0.0480]
Data/restraints/parameters	5130/1/408
Goodness-of-fit on F^2	1.058
Final R indexes [I>=2σ (I)]	R_1 = 0.0368, wR_2 = 0.0966
Final R indexes [all data]	R_1 = 0.0380, wR_2 = 0.0976
Largest diff. peak/hole / e Å^{-3}	0.40/-0.34
Flack parameter	0.028(10)

Fractional Atomic Coordinates (×10^4) and Equivalent Isotropic Displacement Parameters (Å^2×10^3) for EW40755-419-P1B_auto. U_{eq} is defined as 1/3 of the trace of the orthogonalised U_{IJ} tensor.

Atom	*x*	*y*	*z*	U(eq)
S1	7388.8(4)	7307(4)	2775.2(6)	24.92(19)
Cl1	8765.7(4)	8891(4)	1500.4(7)	47.8(3)
O2	8010.7(11)	6809(5)	2877.8(18)	30.7(5)
O1	7144.9(12)	7726(5)	3721.3(17)	30.7(5)
O6	7409.0(12)	-653(5)	5765(2)	36.5(5)
O3	5382.4(12)	6294(5)	3242.3(19)	37.3(6)
O5	5477.8(12)	-615(5)	1260.2(19)	45.3(7)
N5	4897.9(12)	-454(5)	2650(2)	27.0(6)
N4	5463.3(12)	1174(5)	3619(2)	24.7(5)
N3	6256.9(13)	229(5)	4625(2)	30.6(6)
O4	3407.9(12)	-1520(5)	565(2)	45.7(7)
N2	6287.3(13)	5299(5)	3809(2)	28.9(6)
N1	6901.2(13)	6304(5)	2215(2)	26.4(6)
N6	4444.7(14)	-1131(5)	982(2)	37.7(7)
C22	5992.0(15)	1292(5)	4376(2)	25.6(6)
C26	5409.0(15)	-35(5)	3370(2)	25.0(6)
C8	7144.6(16)	5345(5)	1552(3)	27.7(6)
C10	6659.4(16)	4363(5)	1361(2)	29.0(7)
C20	5835.8(16)	3408(5)	4346(2)	27.6(7)
C18	5936.7(16)	6026(5)	3158(2)	27.2(7)
C24	5274.8(17)	3234(5)	3604(3)	31.2(7)
C23	5096.7(15)	2133(5)	3251(3)	28.1(7)
C30	4975.8(16)	-723(5)	1625(3)	30.7(7)
C25	5893.0(17)	-579(5)	3998(3)	30.2(7)
C15	6018.3(17)	4665(6)	1163(2)	31.8(7)
C29	3831.8(15)	-1176(5)	1228(3)	30.4(7)
C21	6179.9(16)	2441(5)	4733(2)	28.4(7)

Fractional Atomic Coordinates (×10^4) and Equivalent Isotropic Displacement Parameters (Å^2×10^3) for EW40755-419-P1B_auto. U_{eq} is defined as 1/3 of the trace of the orthogonalised U_{IJ} tensor.

Atom	*x*	*y*	*z*	U(eq)
C11	6843.7(19)	3177(6)	1359(3)	36.2(8)
C9	7346.1(18)	5801(5)	498(3)	34.7(8)
C17	6220.4(15)	6533(5)	2193(3)	28.0(7)
C1	8353.8(18)	9812(5)	2274(3)	35.1(8)
C7	7359.5(17)	8550(5)	1855(3)	30.0(7)
C19	6048.1(17)	4657(5)	4682(3)	31.0(7)
C6	7725.3(17)	9588(5)	2376(3)	30.0(7)
C2	8671(2)	10800(6)	2783(3)	42.8(9)
C16	5855.1(17)	5975(6)	1182(3)	36.1(8)
C14	5573.4(18)	3763(6)	1014(3)	43.2(9)
C13	5762(2)	2581(6)	996(3)	49.2(11)
C27	4338.4(17)	-893(6)	3101(3)	40.5(9)
C28	3753.6(17)	-716(6)	2322(3)	36.4(8)
C3	8358(2)	11532(5)	3417(3)	46.0(10)
C12	6392(2)	2283(6)	1163(3)	47.3(10)
C4	7733(2)	11328(5)	3526(4)	47.4(9)
O7	5000	7393.29	5000	76.7(17)
C5	7424.9(19)	10374(5)	3004(3)	36.8(8)

Anisotropic Displacement Parameters (Å^2×10^3) for EW40755-419-P1B_auto. The Anisotropic displacement factor exponent takes the form: -2π^2[h^{2}a*^{2}U_{11}+2hka*b*U_{12}+…].

Atom	U_{11}	U_{22}	U_{33}	U_{23}	U_{13}	U_{12}
S1	30.1(4)	25.9(3)	18.0(3)	0.6(3)	0.4(3)	-0.3(3)
Cl1	40.2(5)	72.1(6)	33.6(4)	5.2(4)	14.1(4)	9.6(5)
O2	30.0(12)	32.3(11)	27.8(12)	-2.1(9)	-4.3(10)	-1.3(9)
O1	41.3(13)	29.6(10)	21.9(11)	0.0(9)	6.1(10)	-1.1(10)
O6	35.3(14)	36.0(12)	36.0(13)	1.0(11)	-3.5(11)	5.3(10)
O3	32.2(14)	49.9(14)	30.5(12)	-2.0(11)	6.8(10)	5.6(11)
O5	28.0(13)	85(2)	24.7(12)	-7.1(13)	8.8(10)	-8.6(13)
N5	23.9(14)	38.1(14)	19.5(12)	-0.8(11)	5.1(10)	-6.0(11)
N4	24.3(13)	32.3(14)	17.8(12)	2.1(11)	3.5(10)	-2.2(11)
N3	30.3(15)	34.9(14)	25.5(13)	1.4(12)	-0.1(11)	-0.1(12)
O4	33.2(14)	63.6(18)	37.7(14)	-6.1(13)	-5.0(12)	-8.5(12)
N2	30.9(15)	32.2(13)	23.8(13)	-0.8(11)	4.6(11)	-2.7(12)
N1	26.3(14)	31.0(13)	21.6(12)	-0.4(11)	1.5(10)	0.0(11)
N6	30.7(15)	58.5(19)	24.4(13)	-11.8(14)	4.9(11)	-7.0(14)
C22	25.1(15)	35.8(16)	15.7(13)	1.6(13)	2.0(12)	-2.3(13)
C26	25.9(16)	30.2(15)	19.4(14)	-1.0(12)	4.6(12)	-4.4(12)
C8	26.7(16)	29.7(15)	26.4(15)	-2.1(13)	2.4(13)	0.7(13)

Anisotropic Displacement Parameters ($Å^2×10^3$) for EW40755-419-P1B_auto. The Anisotropic displacement factor exponent takes the form: $-2π^2[h^2a^{*2}U_{11}+2hka^*b^*U_{12}+…]$.

Atom	U_{11}	U_{22}	U_{33}	U_{23}	U_{13}	U_{12}
C10	32.3(18)	35.4(16)	18.3(14)	-1.4(13)	0.4(13)	-3.4(13)
C20	32.8(18)	33.7(16)	17.3(13)	1.3(12)	6.9(13)	-2.3(13)
C18	31.2(18)	29.1(15)	21.5(15)	-7.2(12)	4.4(13)	0.2(13)
C24	31.3(18)	37.4(17)	24.4(15)	2.9(14)	1.2(13)	3.4(14)
C23	25.8(17)	34.8(17)	22.5(15)	2.1(13)	-1.5(13)	1.4(13)
C30	27.0(18)	41.1(17)	24.0(15)	-1.4(13)	3.7(13)	-4.1(13)
C25	34.5(18)	32.2(16)	24.1(15)	-1.4(13)	4.8(14)	-2.1(14)
C15	31.1(18)	47.5(19)	16.3(14)	-4.6(14)	1.4(13)	-4.2(15)
C29	29.1(17)	33.8(16)	27.9(16)	0.1(14)	1.6(14)	-4.4(14)
C21	29.0(16)	38.4(17)	17.5(13)	-0.6(13)	2.6(12)	-5.7(14)
C11	45(2)	34.5(17)	27.8(17)	-4.7(15)	1.0(15)	-4.5(15)
C9	36.5(19)	39.0(17)	30.5(17)	-5.9(15)	10.8(15)	-2.3(14)
C17	24.4(16)	32.0(16)	27.2(15)	1.3(13)	2.4(13)	3.7(12)
C1	34.3(19)	45.8(19)	24.8(16)	13.4(15)	2.2(14)	-0.8(15)
C7	33.1(18)	33.6(16)	22.7(15)	4.9(13)	1.3(13)	-0.5(13)
C19	38.4(19)	35.1(17)	19.8(15)	-2.2(13)	4.9(14)	-2.4(14)
C6	33.5(18)	34.6(17)	21.6(15)	9.4(13)	2.7(13)	1.7(14)
C2	39(2)	54(2)	34.2(19)	17.0(18)	-0.3(16)	-12.3(17)
C16	29.2(18)	57(2)	20.9(15)	2.2(15)	0.4(13)	5.6(16)
C14	35.3(19)	72(3)	23.5(16)	-11.9(18)	6.0(14)	-16.7(19)
C13	56(3)	60(3)	32.9(19)	-12.4(18)	11.5(18)	-29(2)
C27	28.7(18)	67(3)	26.7(16)	0.1(16)	8.0(14)	-14.1(17)
C28	30.1(18)	47.1(19)	33.2(18)	-2.4(15)	9.1(15)	-5.6(15)
C3	68(3)	30.1(17)	39(2)	7.1(16)	3.2(19)	-10.5(17)
C12	66(3)	43.6(19)	32.2(18)	-6.6(17)	6.8(18)	-20(2)
C4	67(3)	27.8(17)	50(2)	2.7(17)	16(2)	-3.1(18)
O7	124(5)	47(2)	68(3)	0	47(3)	0
C5	43(2)	28.6(16)	40.3(19)	7.5(15)	9.9(16)	0.9(15)

Bond Lengths for EW40755-419-P1B_auto.

Atom	Atom	Length/Å	Atom	Atom	Length/Å
S1	O2	1.431(2)	C8	C10	1.509(5)
S1	O1	1.439(2)	C8	C9	1.534(5)
S1	N1	1.629(3)	C10	C15	1.401(5)
S1	C7	1.807(3)	C10	C11	1.386(5)
Cl1	C1	1.734(4)	C20	C24	1.432(5)
O3	C18	1.239(4)	C20	C21	1.363(5)
O5	C30	1.226(4)	C20	C19	1.513(5)
N5	C26	1.404(4)	C18	C17	1.535(4)
N5	C30	1.355(4)	C24	C23	1.348(5)

Bond Lengths for EW40755-419-P1B_auto.

Atom	Atom	Length/Å	Atom	Atom	Length/Å
N5	C27	1.473(4)	C15	C16	1.509(5)
N4	C22	1.385(4)	C15	C14	1.383(5)
N4	C26	1.392(4)	C29	C28	1.499(5)
N4	C23	1.374(4)	C11	C12	1.391(6)
N3	C22	1.337(4)	C17	C16	1.535(5)
N3	C25	1.373(5)	C1	C6	1.388(5)
O4	C29	1.210(4)	C1	C2	1.407(6)
N2	C18	1.317(5)	C7	C6	1.503(5)
N2	C19	1.460(4)	C6	C5	1.394(5)
N1	C8	1.494(4)	C2	C3	1.376(6)
N1	C17	1.473(4)	C14	C13	1.385(7)
N6	C30	1.382(5)	C13	C12	1.375(7)
N6	C29	1.385(4)	C27	C28	1.497(6)
C22	C21	1.405(5)	C3	C4	1.378(7)
C26	C25	1.360(5)	C4	C5	1.375(6)

Bond Angles for EW40755-419-P1B_auto.

Atom	Atom	Atom	Angle/˚	Atom	Atom	Atom	Angle/˚
O2	S1	O1	119.02(14)	C23	C24	C20	121.0(3)
O2	S1	N1	107.67(14)	C24	C23	N4	118.7(3)
O2	S1	C7	108.19(15)	O5	C30	N5	123.8(3)
O1	S1	N1	107.63(14)	O5	C30	N6	120.3(3)
O1	S1	C7	106.99(14)	N5	C30	N6	115.9(3)
N1	S1	C7	106.74(15)	C26	C25	N3	111.6(3)
C26	N5	C27	117.7(3)	C10	C15	C16	117.0(3)
C30	N5	C26	120.4(3)	C14	C15	C10	119.1(4)
C30	N5	C27	119.9(3)	C14	C15	C16	123.8(4)
C22	N4	C26	106.5(3)	O4	C29	N6	120.1(3)
C23	N4	C22	122.3(3)	O4	C29	C28	125.3(3)
C23	N4	C26	131.2(3)	N6	C29	C28	114.5(3)
C22	N3	C25	105.2(3)	C20	C21	C22	119.7(3)
C18	N2	C19	123.1(3)	C10	C11	C12	120.0(4)
C8	N1	S1	119.2(2)	N1	C17	C18	114.3(3)
C17	N1	S1	117.5(2)	N1	C17	C16	109.8(3)
C17	N1	C8	122.0(3)	C16	C17	C18	107.1(3)
C30	N6	C29	127.5(3)	C6	C1	Cl1	120.8(3)
N4	C22	C21	118.7(3)	C6	C1	C2	120.9(4)
N3	C22	N4	111.0(3)	C2	C1	Cl1	118.3(3)
N3	C22	C21	130.3(3)	C6	C7	S1	110.2(2)
N4	C26	N5	120.3(3)	N2	C19	C20	111.5(3)

Bond Angles for EW40755-419-P1B_auto.

Atom	Atom	Atom	Angle/˚	Atom	Atom	Atom	Angle/˚
C25	C26	N5	133.9(3)	C1	C6	C7	123.6(3)
C25	C26	N4	105.7(3)	C1	C6	C5	117.4(3)
N1	C8	C10	109.3(3)	C5	C6	C7	119.0(3)
N1	C8	C9	113.6(3)	C3	C2	C1	119.5(4)
C10	C8	C9	111.7(3)	C15	C16	C17	108.4(3)
C15	C10	C8	119.2(3)	C15	C14	C13	120.3(4)
C11	C10	C8	120.6(3)	C12	C13	C14	120.7(4)
C11	C10	C15	120.2(3)	N5	C27	C28	110.7(3)
C24	C20	C19	120.2(3)	C27	C28	C29	111.8(3)
C21	C20	C24	119.4(3)	C2	C3	C4	120.5(4)
C21	C20	C19	120.4(3)	C13	C12	C11	119.6(4)
O3	C18	N2	124.7(3)	C5	C4	C3	119.5(4)
O3	C18	C17	117.3(3)	C4	C5	C6	122.2(4)
N2	C18	C17	118.0(3)				

Hydrogen Bonds for EW40755-419-P1B_auto.

D	H	A	d(D-H)/Å	d(H-A)/Å	d(D-A)/Å	D-H-A/°
O6	H6A	N3	0.87	2.05	2.858(4)	154.9
O6	H6B	O1[1]	0.87	2.33	3.137(3)	155.4
N2	H2	O6[2]	0.88	2.18	2.964(4)	148.3
N6	H6	O5[3]	0.88	2.20	2.905(4)	136.5
O7	H7C	O3	0.87	1.89	2.747(3)	170.3

[1]+X,-1+Y,+Z; [2]3/2-X,1/2+Y,1-Z; [3]1-X,+Y,-Z

Torsion Angles for EW40755-419-P1B_auto.

A	B	C	D	Angle/˚	A	B	C	D	Angle/˚
S1	N1	C8	C10	165.5(2)	C18	N2	C19	C20	95.4(4)
S1	N1	C8	C9	-68.9(3)	C18	C17	C16	C15	-69.1(3)
S1	N1	C17	C18	-91.4(3)	C24	C20	C21	C22	2.0(4)
S1	N1	C17	C16	148.3(2)	C24	C20	C19	N2	-71.0(4)
S1	C7	C6	C1	94.0(3)	C23	N4	C22	N3	178.2(3)
S1	C7	C6	C5	-85.6(3)	C23	N4	C22	C21	-3.7(4)
Cl1	C1	C6	C7	0.9(4)	C23	N4	C26	N5	-2.2(5)
Cl1	C1	C6	C5	-179.5(3)	C23	N4	C26	C25	-178.3(3)
Cl1	C1	C2	C3	-178.9(3)	C30	N5	C26	N4	102.2(4)
O2	S1	N1	C8	-23.2(3)	C30	N5	C26	C25	-83.0(5)
O2	S1	N1	C17	169.8(2)	C30	N5	C27	C28	-44.9(5)

Torsion Angles for EW40755-419-P1B_auto.

A	B	C	D	Angle/°	A	B	C	D	Angle/°
O2	S1	C7	C6	-72.5(3)	C30	N6	C29	O4	177.4(4)
O1	S1	N1	C8	-152.6(2)	C30	N6	C29	C28	0.2(6)
O1	S1	N1	C17	40.3(3)	C25	N3	C22	N4	0.9(3)
O1	S1	C7	C6	56.9(3)	C25	N3	C22	C21	-176.9(3)
O3	C18	C17	N1	172.8(3)	C15	C10	C11	C12	-0.1(5)
O3	C18	C17	C16	-65.4(4)	C15	C14	C13	C12	2.3(6)
N5	C26	C25	N3	-176.0(3)	C29	N6	C30	O5	-172.0(4)
N5	C27	C28	C29	49.5(4)	C29	N6	C30	N5	7.6(6)
N4	C22	C21	C20	1.0(4)	C21	C20	C24	C23	-2.7(5)
N4	C26	C25	N3	-0.7(3)	C21	C20	C19	N2	108.1(3)
N3	C22	C21	C20	178.7(3)	C11	C10	C15	C16	179.8(3)
O4	C29	C28	C27	153.6(4)	C11	C10	C15	C14	2.8(5)
N2	C18	C17	N1	-10.2(4)	C9	C8	C10	C15	-87.5(4)
N2	C18	C17	C16	111.6(3)	C9	C8	C10	C11	91.3(4)
N1	S1	C7	C6	171.9(2)	C17	N1	C8	C10	-28.0(4)
N1	C8	C10	C15	39.1(4)	C17	N1	C8	C9	97.5(3)
N1	C8	C10	C11	-142.2(3)	C1	C6	C5	C4	-1.1(5)
N1	C17	C16	C15	55.5(4)	C1	C2	C3	C4	-2.2(6)
N6	C29	C28	C27	-29.4(5)	C7	S1	N1	C8	92.8(3)
C22	N4	C26	N5	177.3(3)	C7	S1	N1	C17	-74.2(3)
C22	N4	C26	C25	1.3(3)	C7	C6	C5	C4	178.5(3)
C22	N4	C23	C24	3.1(4)	C19	N2	C18	O3	3.8(5)
C22	N3	C25	C26	-0.1(4)	C19	N2	C18	C17	-173.0(3)
C26	N5	C30	O5	-0.6(5)	C19	C20	C24	C23	176.5(3)
C26	N5	C30	N6	179.8(3)	C19	C20	C21	C22	-177.1(3)
C26	N5	C27	C28	151.1(3)	C6	C1	C2	C3	2.0(5)
C26	N4	C22	N3	-1.4(3)	C2	C1	C6	C7	-179.9(3)
C26	N4	C22	C21	176.7(3)	C2	C1	C6	C5	-0.3(5)
C26	N4	C23	C24	-177.4(3)	C2	C3	C4	C5	0.7(6)
C8	N1	C17	C18	101.9(3)	C16	C15	C14	C13	179.3(3)
C8	N1	C17	C16	-18.4(4)	C14	C15	C16	C17	129.4(3)
C8	C10	C15	C16	-1.4(4)	C14	C13	C12	C11	0.4(6)
C8	C10	C15	C14	-178.4(3)	C27	N5	C26	N4	-93.9(4)
C8	C10	C11	C12	-178.9(3)	C27	N5	C26	C25	80.8(5)
C10	C15	C16	C17	-47.5(4)	C27	N5	C30	O5	-164.1(4)
C10	C15	C14	C13	-3.9(5)	C27	N5	C30	N6	16.3(5)
C10	C11	C12	C13	-1.5(6)	C3	C4	C5	C6	1.0(6)
C20	C24	C23	N4	0.1(5)					

Hydrogen Atom Coordinates (Å×10^4) and Isotropic Displacement Parameters (Å^2×10^3) for EW40755-419-P1B_auto.

Atom	*x*	*y*	*z*	U(eq)
H6A	7114.35	-175.71	5470.68	55
H6B	7456.8	-1170.56	5266.22	55
H2	6684.42	5194.66	3712.51	35
H6	4502.75	-1393.61	342.85	45
H8	7527.41	4996.05	1983.59	33
H24	5024.54	3904	3356.29	37
H23	4724.66	2023.11	2757.68	34
H25	5969.79	-1414	4002.44	36
H21	6545.17	2543.74	5243.48	34
H11	7278.89	2975.43	1491.08	43
H9A	6987.52	6196.43	73.82	52
H9B	7485.93	5127.63	91.56	52
H9C	7693.73	6371.89	656.01	52
H17	6149.7	7415.61	2167.33	34
H7A	7540.72	8308.48	1201.95	36
H7B	6914.86	8789.23	1638.47	36
H19A	5688.04	5101.97	4909.98	37
H19B	6383.77	4609.38	5303.14	37
H2A	9096.92	10959.36	2690.35	51
H16A	5395.27	6075.91	1190.25	43
H16B	5972.17	6374.23	533.7	43
H14	5136.43	3955.19	924.05	52
H13	5452.92	1970.33	867.1	59
H27A	4296.52	-459.63	3774.3	49
H27B	4391.35	-1752.67	3273.83	49
H28A	3649.97	145.04	2273.9	44
H28B	3396.74	-1136.28	2587.04	44
H3	8574.62	12184.39	3782.17	55
H12	6517.33	1470.02	1144.45	57
H4	7517.83	11840.55	3957.21	57
H7C	5142.04	6983.5	4494.74	115
H7D	4753.02	7925.4	4660.76	115
H5	6992.5	10247.27	3074.33	44

Atomic Occupancy for EW40755-419-P1B_auto.

Atom	*Occupancy*	Atom	*Occupancy*	Atom	*Occupancy*
H7C	0.5	H7D	0.5		

Experimental

The crystal was kept at 149.99(10) K during data collection. Using Olex2[69], the structure was solved with the SHELXT[70] structure solution program using Intrinsic Phasing and refined with the SHELXL[71] refinement package using Least Squares minimisation.

Crystal structure determination

Crystal Data for $C_{30}H_{32}ClN_6O_{6.5}S$ (*M* =648.12 g/mol): monoclinic, space group C2 (no. 5), *a* = 21.3601(3) Å, *b* = 11.2017(2) Å, *c* = 12.5762(2) Å, *β* = 97.521(2)°, *V* = 2983.21(8) Å^3, *Z* = 4, *T* = 149.99(10) K, μ(Cu Kα) = 2.272 mm^{-1}, *Dcalc* = 1.443 g/cm^3, 18187 reflections measured (7.09° ≤ 2Θ ≤ 133.17°), 5130 unique (R_{int} = 0.0690, R_{sigma} = 0.0480) which were used in all calculations. The final R_1 was 0.0368 (I > 2σ(I)) and wR_2 was 0.0976 (all data).

Refinement model description

Number of restraints - 1, number of constraints - unknown.
Details:

1. Fixed Uiso

   At 1.2 times of: All C(H) groups, All C(H,H) groups, All N(H) groups

   At 1.5 times of: All C(H,H,H) groups, All O(H,H) groups

   2. Restrained distances O7-O3 2.751 with sigma of 0.01

   3. Others

   Fixed Sof: H7C(0.5) H7D(0.5)

   Fixed X: O7(0.5)

   Fixed Y: O7(0.739329)

   Fixed Z: O7(0.5)

   4.a Free rotating group: O6(H6A,H6B), O7(H7C,H7D)

   4.b Ternary CH refined with riding coordinates: C8(H8), C17(H17)

   4.c Secondary CH2 refined with riding coordinates: C7(H7A,H7B), C19(H19A,H19B), C16(H16A,H16B), C27(H27A,H27B), C28(H28A,H28B)

   4.d Aromatic/amide H refined with riding coordinates: N2(H2), N6(H6), C24(H24), C23(H23), C25(H25), C21(H21), C11(H11), C2(H2A), C14(H14), C13(H13), C3(H3), C12(H12), C4(H4), C5(H5)

   4.e Idealised Me refined as rotating group:

   C9(H9A,H9B,H9C)

MRT-5702C

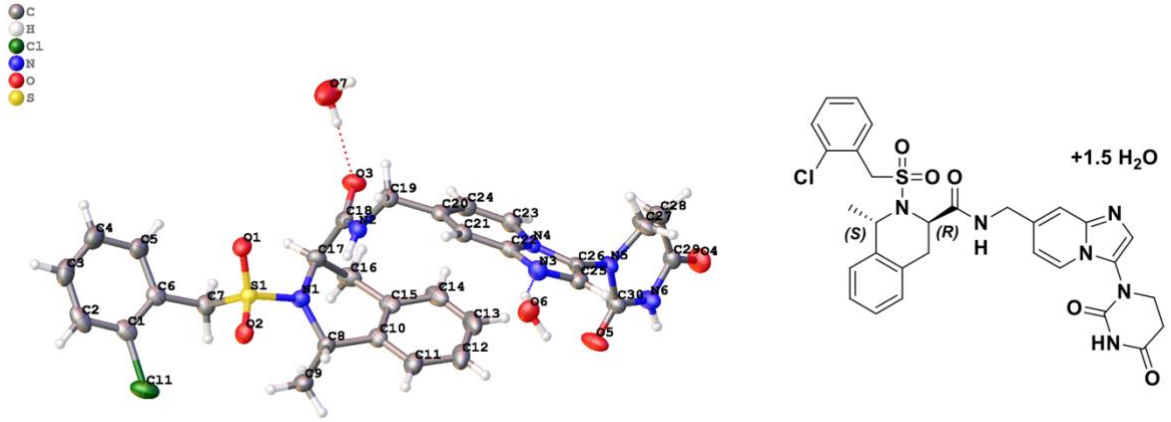

Scheme 4: X-Ray Structure of MRT-5702C (MR-9799) in (*S,R*) configuration.

The symmetry of the crystal structure was assigned the monoclinic space group C2 with the following parameters: a = 21.3441(3) Å, b = 11.1992(2) Å, c = 12.5765(2) Å, α = 90°, β = 97.5310(10)°, γ = 90°, V = 2980.31(8) Å3, Z = 4, Dc = 1.444 g/cm^3, μ(CuKα) = 2.274 mm^{-1}, and F(000) = 1356.0.

Colorless block-shaped single crystals of MRT-5702C were obtained from methanol -water (4:1). A suitable crystal 0.25 × 0.10 × 0.10 mm^3 was selected for testing. Data collection temperature: T = 150.00(10) K. Total of 18726 reflections were collected in the 2θ range from 7.09 to 133.186°. The limiting indices were: -25 ≤ h ≤ 25, -13 ≤ k ≤ 13, -14 ≤ l ≤ 14; which yielded 5178 unique reflections (Rint = 0.0453). The structure was solved using SHELXT (Sheldrick, G. M. 2015. Acta Cryst. A71, 3-8) and refined using SHELXL (against F²) (Sheldrick, G. M. 2015. Acta Cryst. C71, 3-8). The total number of refined parameters was 408, compared with 5178 data. All reflections were included in the refinement. The goodness of fit on F² was 1.047 with a final R value for [I >= 2σ (I)] R_1 = 0.0331 and wR_2 = 0.0847. The largest differential peak and hole were 0.35 and -0.32 eÅ^{-3}.

Crystal data and structure refinement

Empirical formula	$C_{30}H_{32}ClN_6O_{6.5}S$
Formula weight	648.12
Temperature/K	150.00(10)
Crystal system	monoclinic
Space group	C2
a/Å	21.3441(3)
b/Å	11.1992(2)
c/Å	12.5765(2)
α/°	90
β/°	97.5310(10)
γ/°	90
Volume/Å^3	2980.31(8)
Z	4
ρ_{calc}g/cm^3	1.444
μ/mm^{-1}	2.274
F(000)	1356.0
Crystal size/mm^3	0.25 × 0.1 × 0.1
Radiation	Cu Kα (λ = 1.54184)
2Θ range for data collection/°	7.09 to 133.186
Index ranges	-25 ≤ h ≤ 25, -13 ≤ k ≤ 13, -14 ≤ l ≤ 14
Reflections collected	18726
Independent reflections	5178 [R_{int} = 0.0453, R_{sigma} = 0.0382]
Data/restraints/parameters	5178/2/408
Goodness-of-fit on F^2	1.047
Final R indexes [I>=2σ (I)]	R_1 = 0.0331, wR_2 = 0.0847
Final R indexes [all data]	R_1 = 0.0342, wR_2 = 0.0856
Largest diff. peak/hole / e Å^{-3}	0.35/-0.32
Flack parameter	-0.011(8)

Fractional Atomic Coordinates (×10^4) and Equivalent Isotropic Displacement Parameters (Å^2×10^3) for EW40755-419-P3B_auto. U_{eq} is defined as 1/3 of the trace of the orthogonalised U_{IJ} tensor.

Atom	*x*	*y*	*z*	U(eq)
S1	2611.6(3)	2705(3)	7224.5(5)	23.98(17)
Cl1	1234.8(4)	1123(4)	8499.8(7)	47.4(2)
O2	1988.9(10)	3202(4)	7122.0(18)	29.8(5)
O1	2854.6(10)	2285(4)	6279.4(17)	30.2(5)
O6	2590.1(11)	10663(4)	4231.4(19)	35.8(5)
O3	4617.2(10)	3719(4)	6755.9(16)	36.8(6)
O5	4522.9(10)	10623(5)	8739.4(18)	44.1(7)
N5	5102.4(11)	10465(4)	7348.3(19)	25.7(5)
N4	4536.1(11)	8839(4)	6383.0(19)	23.0(5)
O4	6592.7(11)	11531(4)	9433(2)	44.9(7)
N3	3744.8(12)	9783(4)	5379(2)	29.7(6)

Fractional Atomic Coordinates (×10^4) and Equivalent Isotropic Displacement Parameters (Å^2×10^3) for EW40755-419-P3B_auto. U_{eq} is defined as 1/3 of the trace of the orthogonalised U_{IJ} tensor.

Atom	*x*	*y*	*z*	U(eq)
N2	3711.9(12)	4714(4)	6191(2)	27.4(6)
N6	5557.6(12)	11143(5)	9017(2)	37.3(7)
N1	3097.8(11)	3704(4)	7786(2)	25.7(5)
C22	4006.7(13)	8721(5)	5625(2)	24.9(6)
C26	4590.8(13)	10045(4)	6627(2)	25.0(6)
C8	2855.7(14)	4665(5)	8450(3)	26.4(6)
C10	3340.3(14)	5646(5)	8641(2)	28.2(7)
C30	5021.3(14)	10731(5)	8374(2)	29.8(7)
C23	4902.4(14)	7877(5)	6745(2)	28.2(7)
C24	4726.6(15)	6778(5)	6394(3)	30.5(7)
C20	4165.7(14)	6605(5)	5653(2)	26.4(6)
C21	3821.1(14)	7573(5)	5268(2)	26.9(6)
C18	4062.5(14)	3987(5)	6844(2)	26.6(6)
C29	6167.7(14)	11185(5)	8773(3)	29.7(7)
C15	3979.6(15)	5349(5)	8836(2)	31.3(7)
C9	2654.2(16)	4210(5)	9500(3)	33.7(7)
C7	2638.7(15)	1466(5)	8141(2)	29.4(7)
C11	3155.7(17)	6834(5)	8642(3)	36.3(7)
C1	1645.1(15)	198(5)	7723(3)	33.2(7)
C6	2274.7(15)	424(5)	7625(2)	29.0(7)
C17	3779.8(14)	3480(5)	7805(3)	27.7(7)
C25	4107.8(15)	10588(5)	6002(2)	28.7(7)
C2	1329.7(17)	-784(5)	7214(3)	42.7(9)
C16	4143.8(15)	4041(5)	8819(3)	34.7(8)
C19	3952.7(16)	5358(5)	5318(3)	30.6(7)
C14	4425.4(16)	6247(5)	8985(3)	43.2(9)
C13	4237.9(19)	7432(5)	9004(3)	49.0(10)
C28	6244.8(15)	10736(5)	7680(3)	34.3(7)
C27	5662.6(15)	10900(5)	6900(3)	40.9(9)
O7	5000	2612.71	5000	80.2(16)
C12	3608(2)	7728(5)	8837(3)	45.0(9)
C3	1642(2)	-1521(5)	6579(3)	45.5(9)
C4	2264(2)	-1315(5)	6474(3)	46.8(9)
C5	2577.6(17)	-365(5)	6995(3)	35.8(7)

Anisotropic Displacement Parameters (Å^2×10^3) for EW40755-419-P3B_auto. The Anisotropic displacement factor exponent takes the form: -2π^2[h^{2}a*^{2}U_{11}+2hka*b*U_{12}+…].

Atom	U_{11}	U_{22}	U_{33}	U_{23}	U_{13}	U_{12}
S1	25.8(3)	25.9(3)	18.7(3)	0.5(3)	-2.9(3)	-0.2(3)

Anisotropic Displacement Parameters ($Å^2×10^3$) for EW40755-419-P3B_auto. The Anisotropic displacement factor exponent takes the form: $-2π^2[h^2a^{*2}U_{11}+2hka^*b^*U_{12}+…]$.

Atom	U_{11}	U_{22}	U_{33}	U_{23}	U_{13}	U_{12}
Cl1	36.0(4)	73.9(7)	34.3(4)	5.1(4)	11.3(3)	9.6(4)
O2	26.4(10)	31.8(11)	28.1(11)	-2.2(9)	-7.4(9)	-1.4(9)
O1	38.4(11)	30.7(11)	21.1(11)	-0.6(9)	2.3(9)	-1.2(9)
O6	31.0(12)	35.8(13)	37.6(13)	0.0(10)	-6.3(10)	6.0(10)
O3	27.5(11)	50.4(15)	32.8(12)	-1.7(11)	4.6(9)	5.8(11)
O5	23.6(11)	84(2)	25.6(12)	-6.8(12)	5.4(9)	-8.1(12)
N5	20.9(12)	36.3(15)	19.6(12)	-1.0(11)	1.8(9)	-6.1(11)
N4	18.7(11)	32.4(14)	17.4(12)	2.6(11)	0.8(9)	-2.4(10)
O4	28.4(12)	62.6(18)	40.0(14)	-6.7(12)	-9.0(10)	-9.1(11)
N3	25.5(12)	35.7(15)	25.9(13)	1.9(11)	-4.0(10)	-0.6(11)
N2	26.3(12)	32.3(14)	23.3(13)	-1.3(11)	1.7(10)	-3.1(11)
N6	27.9(13)	58.4(19)	25.0(13)	-11.4(13)	1.4(10)	-8.0(14)
N1	22.7(12)	30.9(14)	22.6(12)	-1.0(11)	-1.0(9)	1.4(11)
C22	19.8(12)	38.6(17)	15.5(13)	2.5(13)	-0.6(11)	-1.7(13)
C26	21.0(13)	32.7(17)	21.3(14)	-2.7(12)	2.7(11)	-5.2(12)
C8	22.7(13)	27.8(16)	27.1(15)	-2.2(13)	-2.1(11)	2.3(12)
C10	28.7(15)	36.9(17)	17.4(14)	-2.7(13)	-3.0(11)	-3.6(13)
C30	23.8(15)	40.2(18)	24.8(15)	-1.8(13)	0.9(12)	-3.6(13)
C23	22.0(14)	36.2(18)	24.3(15)	2.6(13)	-4.2(11)	-0.9(12)
C24	26.1(14)	38.4(18)	25.9(16)	3.2(14)	-0.7(12)	3.3(13)
C20	28.6(15)	33.5(17)	17.2(13)	-1.0(12)	3.2(11)	-2.9(12)
C21	23.4(13)	37.8(18)	18.6(13)	0.7(13)	-0.9(11)	-3.5(13)
C18	26.9(15)	30.2(16)	21.6(15)	-6.6(12)	-0.6(11)	-2.6(12)
C29	24.9(14)	32.2(17)	30.6(16)	0.8(14)	-1.4(12)	-2.8(13)
C15	28.8(15)	48(2)	15.9(14)	-5.6(13)	-2.2(12)	-5.2(14)
C9	33.5(16)	37.7(18)	31.0(17)	-6.7(14)	8.0(14)	-2.0(14)
C7	30.1(15)	33.0(18)	23.5(15)	4.1(13)	-1.7(12)	-2.9(13)
C11	42.2(18)	35.0(18)	30.1(18)	-4.0(15)	-1.6(13)	-5.9(15)
C1	31.8(16)	43.4(19)	23.0(16)	12.9(14)	-1.2(12)	0.6(14)
C6	31.6(15)	33.3(18)	20.6(15)	8.0(13)	-1.7(12)	1.6(13)
C17	22.1(14)	33.1(17)	26.9(15)	0.9(13)	-0.1(11)	3.3(12)
C25	30.1(15)	31.2(17)	24.7(15)	-0.3(13)	3.5(12)	-1.1(13)
C2	35.9(18)	55(2)	34.2(19)	20.1(17)	-5.0(15)	-13.0(17)
C16	23.6(15)	57(2)	22.1(15)	1.7(15)	-3.3(12)	5.1(14)
C19	36.1(17)	34.4(18)	20.8(15)	-0.9(13)	2.0(12)	-3.2(14)
C14	32.2(16)	72(3)	25.6(16)	-13.7(18)	3.8(13)	-17.6(18)
C13	53(2)	60(3)	35.5(19)	-14.8(18)	9.3(17)	-29.8(19)
C28	24.6(15)	45(2)	33.6(17)	-0.9(15)	4.9(13)	-3.4(13)
C27	24.0(15)	72(3)	27.7(17)	0.6(17)	5.4(13)	-13.5(16)
O7	129(5)	50(3)	72(3)	0	50(3)	0
C12	62(2)	39.9(19)	33.1(18)	-6.0(17)	4.2(16)	-19.1(19)

Anisotropic Displacement Parameters ($Å^2×10^3$) for EW40755-419-P3B_auto. The Anisotropic displacement factor exponent takes the form: $-2π^2[h^2a^{*2}U_{11}+2hka^*b^*U_{12}+…]$.

Atom	U_{11}	U_{22}	U_{33}	U_{23}	U_{13}	U_{12}
C3	63(2)	29.9(19)	42(2)	5.2(16)	-0.7(18)	-10.2(17)
C4	63(2)	29.3(19)	50(2)	1.5(17)	12.4(18)	0.1(18)
C5	39.8(18)	27.2(17)	41.3(19)	6.5(15)	8.1(14)	2.0(14)

Bond Lengths for EW40755-419-P3B_auto.

Atom	Atom	Length/Å	Atom	Atom	Length/Å
S1	O2	1.431(2)	C8	C10	1.507(4)
S1	O1	1.437(2)	C8	C9	1.528(5)
S1	N1	1.624(3)	C10	C15	1.395(4)
S1	C7	1.801(3)	C10	C11	1.388(5)
Cl1	C1	1.738(4)	C23	C24	1.344(5)
O3	C18	1.240(4)	C24	C20	1.431(4)
O5	C30	1.219(4)	C20	C21	1.364(5)
N5	C26	1.406(4)	C20	C19	1.511(5)
N5	C30	1.357(4)	C18	C17	1.530(4)
N5	C27	1.471(4)	C29	C28	1.494(5)
N4	C22	1.386(4)	C15	C16	1.507(5)
N4	C26	1.387(4)	C15	C14	1.380(5)
N4	C23	1.374(4)	C7	C6	1.501(5)
O4	C29	1.210(4)	C11	C12	1.391(5)
N3	C22	1.332(4)	C1	C6	1.389(5)
N3	C25	1.367(4)	C1	C2	1.399(6)
N2	C18	1.318(4)	C6	C5	1.400(5)
N2	C19	1.462(4)	C17	C16	1.537(5)
N6	C30	1.391(4)	C2	C3	1.379(6)
N6	C29	1.377(4)	C14	C13	1.387(7)
N1	C8	1.495(4)	C13	C12	1.374(6)
N1	C17	1.474(4)	C28	C27	1.490(5)
C22	C21	1.402(5)	C3	C4	1.372(6)
C26	C25	1.355(4)	C4	C5	1.377(6)

Bond Angles for EW40755-419-P3B_auto.

Atom	Atom	Atom	Angle/˚	Atom	Atom	Atom	Angle/˚
O2	S1	O1	118.99(13)	C21	C20	C24	119.3(3)
O2	S1	N1	107.70(13)	C21	C20	C19	120.5(3)
O2	S1	C7	108.01(15)	C20	C21	C22	119.9(3)

Bond Angles for EW40755-419-P3B_auto.

Atom	Atom	Atom	Angle/˚	Atom	Atom	Atom	Angle/˚
O1	S1	N1	107.82(13)	O3	C18	N2	124.4(3)
O1	S1	C7	107.00(14)	O3	C18	C17	117.4(3)
N1	S1	C7	106.72(14)	N2	C18	C17	118.1(3)
C26	N5	C27	117.7(3)	O4	C29	N6	120.3(3)
C30	N5	C26	120.1(2)	O4	C29	C28	125.2(3)
C30	N5	C27	120.2(3)	N6	C29	C28	114.5(3)
C22	N4	C26	106.4(2)	C10	C15	C16	116.9(3)
C23	N4	C22	122.1(3)	C14	C15	C10	119.4(4)
C23	N4	C26	131.5(3)	C14	C15	C16	123.6(3)
C22	N3	C25	105.4(2)	C6	C7	S1	110.5(2)
C18	N2	C19	123.1(3)	C10	C11	C12	120.0(4)
C29	N6	C30	127.7(3)	C6	C1	Cl1	120.4(3)
C8	N1	S1	119.4(2)	C6	C1	C2	121.1(3)
C17	N1	S1	117.6(2)	C2	C1	Cl1	118.5(3)
C17	N1	C8	121.8(2)	C1	C6	C7	123.7(3)
N4	C22	C21	118.6(3)	C1	C6	C5	117.3(3)
N3	C22	N4	110.8(3)	C5	C6	C7	118.9(3)
N3	C22	C21	130.6(3)	N1	C17	C18	114.5(2)
N4	C26	N5	120.3(3)	N1	C17	C16	109.5(3)
C25	C26	N5	133.8(3)	C18	C17	C16	107.2(3)
C25	C26	N4	105.8(3)	C26	C25	N3	111.6(3)
N1	C8	C10	109.5(2)	C3	C2	C1	119.6(3)
N1	C8	C9	113.6(3)	C15	C16	C17	108.4(3)
C10	C8	C9	111.8(3)	N2	C19	C20	111.7(3)
C15	C10	C8	119.3(3)	C15	C14	C13	120.3(3)
C11	C10	C8	120.7(3)	C12	C13	C14	120.5(3)
C11	C10	C15	120.0(3)	C27	C28	C29	112.4(3)
O5	C30	N5	124.3(3)	N5	C27	C28	110.9(3)
O5	C30	N6	120.4(3)	C13	C12	C11	119.7(4)
N5	C30	N6	115.3(3)	C4	C3	C2	120.2(4)
C24	C23	N4	119.1(3)	C3	C4	C5	120.0(4)
C23	C24	C20	120.8(3)	C4	C5	C6	121.7(3)
C24	C20	C19	120.2(3)				

Hydrogen Bonds for EW40755-419-P3B_auto.

D	H	A	d(D-H)/Å	d(H-A)/Å	d(D-A)/Å	D-H-A/°
O6	H6A	N3	0.87	2.02	2.863(3)	162.6
O6	H6B	O1[1]	0.87	2.34	3.142(3)	152.8
N2	H2	O6[2]	0.88	2.17	2.958(4)	148.5
N6	H6	O5[3]	0.88	2.21	2.908(4)	136.3

Hydrogen Bonds for EW40755-419-P3B_auto.

D	H	A	d(D-H)/Å	d(H-A)/Å	d(D-A)/Å	D-H-A/°
O7	H7C	O3	0.87	1.88	2.7479(14)	171.8
O7	H7D	O3[4]	0.87	1.95	2.7479(14)	152.8

[1]+X,1+Y,+Z; [2]1/2-X,-1/2+Y,1-Z; [3]1-X,+Y,2-Z; [4]1-X,+Y,1-Z

Torsion Angles for EW40755-419-P3B_auto.

A	B	C	D	Angle/°	A	B	C	D	Angle/°
S1	N1	C8	C10	-165.3(2)	C30	N5	C26	C25	82.9(4)
S1	N1	C8	C9	69.0(3)	C30	N5	C27	C28	44.2(5)
S1	N1	C17	C18	91.1(3)	C30	N6	C29	O4	-177.4(4)
S1	N1	C17	C16	-148.5(2)	C30	N6	C29	C28	0.4(6)
S1	C7	C6	C1	-93.8(3)	C23	N4	C22	N3	-177.9(3)
S1	C7	C6	C5	85.3(3)	C23	N4	C22	C21	3.8(4)
Cl1	C1	C6	C7	-1.5(4)	C23	N4	C26	N5	1.5(5)
Cl1	C1	C6	C5	179.4(2)	C23	N4	C26	C25	178.0(3)
Cl1	C1	C2	C3	178.9(3)	C23	C24	C20	C21	2.7(5)
O2	S1	N1	C8	23.0(3)	C23	C24	C20	C19	-176.2(3)
O2	S1	N1	C17	-169.5(2)	C24	C20	C21	C22	-2.1(4)
O2	S1	C7	C6	72.6(3)	C24	C20	C19	N2	71.1(4)
O1	S1	N1	C8	152.6(2)	C21	C20	C19	N2	-107.9(3)
O1	S1	N1	C17	-40.0(3)	C18	N2	C19	C20	-95.2(4)
O1	S1	C7	C6	-56.6(3)	C18	C17	C16	C15	68.9(3)
O3	C18	C17	N1	-172.5(3)	C29	N6	C30	O5	171.8(4)
O3	C18	C17	C16	65.8(4)	C29	N6	C30	N5	-7.8(6)
N5	C26	C25	N3	176.2(3)	C29	C28	C27	N5	-48.7(5)
N4	C22	C21	C20	-1.0(4)	C15	C10	C11	C12	0.1(5)
N4	C26	C25	N3	0.5(3)	C15	C14	C13	C12	-2.3(5)
N4	C23	C24	C20	-0.1(5)	C9	C8	C10	C15	87.6(3)
O4	C29	C28	C27	-153.7(4)	C9	C8	C10	C11	-91.2(4)
N3	C22	C21	C20	-179.0(3)	C7	S1	N1	C8	-92.7(2)
N2	C18	C17	N1	10.2(4)	C7	S1	N1	C17	74.7(2)
N2	C18	C17	C16	-111.5(3)	C7	C6	C5	C4	-178.0(3)
N6	C29	C28	C27	28.6(5)	C11	C10	C15	C16	-179.8(3)
N1	S1	C7	C6	-171.9(2)	C11	C10	C15	C14	-2.7(5)
N1	C8	C10	C15	-39.1(4)	C1	C6	C5	C4	1.2(5)
N1	C8	C10	C11	142.1(3)	C1	C2	C3	C4	2.1(6)
N1	C17	C16	C15	-55.8(3)	C6	C1	C2	C3	-2.0(5)
C22	N4	C26	N5	-177.5(2)	C17	N1	C8	C10	27.8(4)
C22	N4	C26	C25	-1.0(3)	C17	N1	C8	C9	-97.9(3)
C22	N4	C23	C24	-3.2(4)	C25	N3	C22	N4	-0.9(3)
C22	N3	C25	C26	0.3(3)	C25	N3	C22	C21	177.1(3)
C26	N5	C30	O5	0.6(5)	C2	C1	C6	C7	179.5(3)

Torsion Angles for EW40755-419-P3B_auto.

A	B	C	D	Angle/°	A	B	C	D	Angle/°
C26	N5	C30	N6	-179.7(3)	C2	C1	C6	C5	0.3(5)
C26	N5	C27	C28	-151.6(3)	C2	C3	C4	C5	-0.6(6)
C26	N4	C22	N3	1.2(3)	C16	C15	C14	C13	-179.2(3)
C26	N4	C22	C21	-177.1(3)	C19	N2	C18	O3	-4.2(5)
C26	N4	C23	C24	177.9(3)	C19	N2	C18	C17	172.9(3)
C8	N1	C17	C18	-101.8(3)	C19	C20	C21	C22	176.9(3)
C8	N1	C17	C16	18.6(4)	C14	C15	C16	C17	-129.2(3)
C8	C10	C15	C16	1.3(4)	C14	C13	C12	C11	-0.3(6)
C8	C10	C15	C14	178.4(3)	C27	N5	C26	N4	94.0(4)
C8	C10	C11	C12	178.9(3)	C27	N5	C26	C25	-81.2(5)
C10	C15	C16	C17	47.8(4)	C27	N5	C30	O5	164.4(4)
C10	C15	C14	C13	3.8(5)	C27	N5	C30	N6	-16.0(5)
C10	C11	C12	C13	1.5(6)	C3	C4	C5	C6	-1.1(6)
C30	N5	C26	N4	-101.8(4)					

Hydrogen Atom Coordinates (Å×10^4) and Isotropic Displacement Parameters (Å^2×10^3) for EW40755-419-P3B_auto.

Atom	*x*	*y*	*z*	U(eq)
H6A	2912.83	10250.13	4522.87	54
H6B	2535.37	11204.65	4705.96	54
H2	3314.06	4816.04	6284.13	33
H6	5500.15	11407.85	9656.03	45
H8	2472.6	5014.31	8019.01	32
H23	5275.17	7986.24	7237.82	34
H24	4977.89	6108.21	6640.34	37
H21	3455.62	7470.32	4757.33	32
H9A	2309.22	3633.67	9342.09	51
H9B	2510.02	4883.49	9902.9	51
H9C	3014.06	3822.58	9928.46	51
H7A	3083.65	1227.88	8360.22	35
H7B	2456.37	1708.82	8792.52	35
H11	2720.22	7036.07	8509.48	44
H17	3852.27	2597.34	7831.63	33
H25	4030.96	11423.39	5998.34	34
H2A	902.87	-942.51	7306.2	51
H16A	4025.85	3641.88	9466.43	42
H16B	4604.2	3941.64	8812.9	42
H19A	3617.25	5405.3	4696.57	37
H19B	4312.99	4911.42	5091.12	37
H14	4862.47	6053.32	9075.22	52
H13	4547.17	8043.25	9133.8	59

Hydrogen Atom Coordinates (Å×10^4) and Isotropic Displacement Parameters (Å^2×10^3) for EW40755-419-P3B_auto.

Atom	*x*	*y*	*z*	U(eq)
H28A	6599.58	11163.98	7415.06	41
H28B	6353.61	9876.26	7725.12	41
H27A	5608.34	11757.87	6719.33	49
H27B	5706.73	10460	6231.1	49
H7C	4849.8	2996.32	5512.54	120
H7D	5079.82	3166.57	4551.72	120
H12	3482.17	8540.84	8854.78	54
H3	1425.23	-2172.25	6213.05	55
H4	2479.26	-1828.84	6041.24	56
H5	3010.59	-240.38	6925.55	43

Atomic Occupancy for EW40755-419-P3B_auto.

Atom	*Occupancy*	Atom	*Occupancy*	Atom	*Occupancy*
H7C	0.5	H7D	0.5		

Experimental

The crystal was kept at 150.00(10) K during data collection. Using Olex2[69], the structure was solved with the SHELXT[70] structure solution program using Intrinsic Phasing and refined with the SHELXL[71] refinement package using Least Squares minimization.

Crystal structure determination

Crystal Data for $C_{30}H_{32}ClN_6O_{6.5}S$ (*M* =648.12 g/mol): monoclinic, space group C2 (no. 5), *a* = 21.3441(3) Å, *b* = 11.1992(2) Å, *c* = 12.5765(2) Å, *β* = 97.5310(10)°, *V* = 2980.31(8) Å^3, *Z* = 4, *T* = 150.00(10) K, μ(Cu Kα) = 2.274 mm^{-1}, *Dcalc* = 1.444 g/cm^3, 18726 reflections measured (7.09° ≤ 2Θ ≤ 133.186°), 5178 unique (R_{int} = 0.0453, R_{sigma} = 0.0382) which were used in all calculations. The final R_1 was 0.0331 (I > 2σ(I)) and wR_2 was 0.0856 (all data).

Refinement model description

Number of restraints - 2, number of constraints - unknown.

Details:

1. Fixed Uiso

At 1.2 times of:

All C(H) groups, All C(H,H) groups, All N(H) groups

At 1.5 times of:

All C(H,H,H) groups, All O(H,H) groups

2. Restrained distances

O3-O7

2.748 with sigma of 0.001

O3-H7C

1.884 with sigma of 0.001

3. Others

Fixed Sof: H7C(0.5) H7D(0.5)

Fixed X: O7(0.5)

Fixed Y: O7(0.261271)

Fixed Z: O7(0.5)

4.a Free rotating group:

O6(H6A,H6B), O7(H7C,H7D)

4.b Ternary CH refined with riding coordinates:

C8(H8), C17(H17)

4.c Secondary CH2 refined with riding coordinates:

C7(H7A,H7B), C16(H16A,H16B), C19(H19A,H19B), C28(H28A,H28B), C27(H27A,H27B)

4.d Aromatic/amide H refined with riding coordinates:

N2(H2), N6(H6), C23(H23), C24(H24), C21(H21), C11(H11), C25(H25), C2(H2A), C14(H14), C13(H13), C12(H12), C3(H3), C4(H4), C5(H5)

4.e Idealised Me refined as rotating group:

C9(H9A,H9B,H9C)

Supplementary Methods References

59. Huang, T. et al. MSstatsTMT: Statistical Detection of Differentially Abundant Proteins in Experiments with Isobaric Labeling and Multiple Mixtures. *Mol Cell Proteomics* **19**, 1706-1723 (2020).
60. Tsai, T.H. et al. Selection of Features with Consistent Profiles Improves Relative Protein Quantification in Mass Spectrometry Experiments. *Mol Cell Proteomics* **19**, 944-959 (2020).

61. Phipson, B., Lee, S., Majewski, I.J., Alexander, W.S. & Smyth, G.K. Robust Hyperparameter Estimation Protects against Hypervariable Genes and Improves Power to Detect Differential Expression. *Ann Appl Stat* **10**, 946-963 (2016).
62. Ritchie, M.E. et al. limma powers differential expression analyses for RNA-sequencing and microarray studies. *Nucleic Acids Res* **43**, e47 (2015).
63. Zhou, Q. PyMesh—Geometry Processing Library for Python (2019).
64. Jurrus, E. et al. Improvements to the APBS biomolecular solvation software suite. *Protein Sci* **27**, 112-128 (2018).
65. Lawrence, M.C. & Colman, P.M. Shape complementarity at protein/protein interfaces. *J Mol Biol* **234**, 946-50 (1993).
66. Hawkins, P.C., Skillman, A.G., Warren, G.L., Ellingson, B.A. & Stahl, M.T. Conformer generation with OMEGA: algorithm and validation using high quality structures from the Protein Databank and Cambridge Structural Database. *J Chem Inf Model* **50**, 572-84 (2010).
67. Buttenschoen, M., Morris, G.M. & Deane, C.M. PoseBusters: AI-based docking methods fail to generate physically valid poses or generalise to novel sequences. *Chem Sci* **15**, 3130-3139 (2024).
68. Joseph, A.P. et al. Refinement of atomic models in high resolution EM reconstructions using Flex-EM and local assessment. *Methods* **100**, 42-9 (2016).
69. Cragnolini, T. et al. TEMPy2: a Python library with improved 3D electron microscopy density-fitting and validation workflows. *Acta Crystallogr D Struct Biol* **77**, 41-47 (2021).
70. Waskom, M. seaborn: statistical data visualization. *Journal of Open Source Software* **6**(2021).